PHYSICAL REVIEW SPECIAL TOPICS - ACCELERATORS AND BEAMS **8**, 102802 (2005)

Method of phase-space tomography of rapidly evolving *E* beams

K. Chalut
Department of Physics, Duke University, Durham, North Carolina 27708, USA

V. N. Litvinenko and I. V. Pinayev
Brookhaven National Laboratory, Upton, New York 11973, USA

(Received 22 January 2005; published 25 October 2005)

In this paper, we describe a new method of phase-space tomography. This method allows one to restore phase-space density using a small number of projections covering a limited range of linear transformations in the phase space. Practical applications of this method are discussed.

DOI: 10.1103/PhysRevSTAB.8.102802 PACS numbers: 41.60.Cr

I. INTRODUCTION

There have been quite a few ideas about how to reconstruct a distribution given a limited set of data (see [1] for description of the filtered-backprojection algorithm, [2] for description of the Algebraic Reconstruction Technique, and [3] for a method which uses the principle of maximum entropy). All of these methods suffer from limitations in the consideration of the phase-space reconstruction problem when given a limited set of profiles, however. We set out to find a method of tomography that was fast, efficient, accurate, and also had no limitations governing its use, i.e., it does not require evenly spread angles, it can be used for N-dimensional distributions, and it will work for any linear phase-space transformation. Certain processes evolve on the same time scale as the temporal spacing of their linear projections, e.g., the synchrotron oscillation period of particles (rotation in phase space). They therefore necessitate a very flexible yet accurate method of phase-space tomography in order to reconstruct its phase-space density from a limited number of projections covering a small angle of rotation. One such process is the evolution of the electron beam distribution during the giant pulse process in storage ring (SR) free electron lasers (FEL).

In the giant pulse process in a storage ring FEL [4], the electron beam evolves dramatically and its energy spread increases by up to a factor of 3 within one synchrotron oscillation. The restoration of the evolution of giant pulses, and other processes that evolve quickly, requires a new method of reconstruction. We investigate a new method of phase-space reconstruction that is not limited by observation angle, and works for any linear transformation, not just rotation. The only requirement is that we have some known set of linear projections.

II. METHOD DESCRIPTION

A. Projection matrix

Suppose we have an arbitrary distribution function of particles $F(\vec{X}_n, \vec{P}_n)$ in an N^D phase space (D is its dimension), described by its spatial ($\vec{X}$) and canonical momentum ($\vec{P}$) coordinates. F can be expanded by a set of basis functions:

$$F(\vec{x}) = a_{k,l,\ldots}\chi_{k,l,\ldots}(\vec{x}), \tag{1}$$

where $\vec{x} = (x_1, p_1, \ldots, x_N, p_N)$. Taking the Radon transform of each side [1], we can define a projection operator $\hat{P}(\alpha)$ which, when acting upon the distribution, will give us a set of linear projections (images) $I(\vec{x}_m, \alpha)$ which satisfy the tensorial relationship

$$I(\vec{x}_m, \alpha) = \hat{P}(\alpha) \otimes F(\vec{X}_n, \vec{P}_n). \tag{2}$$

$\vec{x}_m$ is the subset of spatial coordinates in the projection (image) space. The typical projection space used for imaging a beam of charged particles has one or two dimensions. The projection matrix depends only upon the parameter α, which we use to identify the projection.

The method is applicable to any process with linear transformations and projections [5]. In our specific example we used a dual-sweep streak camera [6] (hence the one dimensional images) for reconstruction of an evolution of electron beam density (F) in longitudinal phase space (two dimensions) (see Fig. 1).

The longitudinal phase space of an electron beam in a storage ring can be described by two dimensionless coordinates $\varepsilon = (E - E_0)/\sigma_{E0}$ and $\zeta = (t - t_0)/\sigma_{t0}$, where E and t are the energy and arrival time of an electron, E_0 and t_0 are, respectively, the energy and time of the synchronous electron, and σ_{E0} and σ_{t0} are corresponding rms spreads of a stationary beam. The electron bunches under study are very short and the unperturbed motions of the electrons in the longitudinal phase space can be represented as a simple rotation in which the angle in question is the synchrotron phase advance φ

$$\begin{bmatrix} \varepsilon \\ \zeta \end{bmatrix}_n = \begin{bmatrix} \cos\varphi_n & \sin\varphi_n \\ -\sin\varphi_n & \cos\varphi_n \end{bmatrix} \cdot \begin{bmatrix} \varepsilon \\ \zeta \end{bmatrix}_o; \qquad \varphi_n = n \cdot 2\pi Q_s, \tag{3}$$

where $Q_s \ll 1$ is synchrotron tune [7] and n is the turn number. The rotation causes a transformation of the phase-

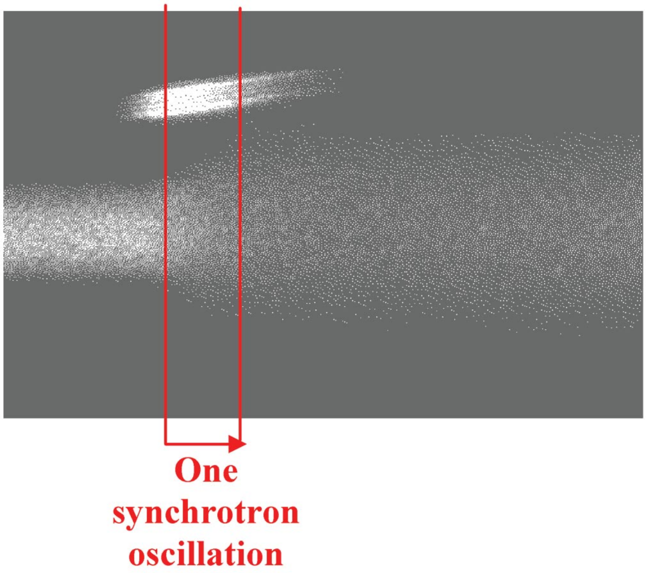

FIG. 1. (Color) Dual-sweep streak-camera image of giant pulse. The camera recorded the time structure of the intensity of the light generated by the E beam on multiple turns. The fast vertical sweep, which is synchronized with the revolution of the E beam, has the full scale of 1.6 nsec. The slow horizontal sweep has the full scale of 500 msec. The trace seen at top is the FEL light. The main image is that of the spontaneous radiation of electron beam, which is identical to the beam time profile.

space density governed by the Liouville theorem:

$$F_n(\zeta, \varepsilon) = F_0(\zeta \cdot \cos\varphi_n + \varepsilon \cdot \sin\varphi_n, \varepsilon \cdot \cos\varphi_n - \zeta \cdot \sin\varphi_n). \tag{4}$$

At each turn of the E beam around the ring the dual-sweep streak-camera records the time profile of the beam, i.e., the projection of the phase-space density $F(\zeta, \epsilon,)$ onto the time coordinate:

$$\begin{aligned} I(\zeta \cdot \sigma_{to})_\varphi &= P(\varphi) \otimes F_0(\zeta, \varepsilon) = \int_{-\infty}^{\infty} F(\zeta', \varepsilon') \cdot d\varepsilon \\ &= \int_{-\infty}^{\infty} F_0(\zeta \cdot \cos\varphi_n + \varepsilon \cdot \sin\varphi_n, \varepsilon \cdot \cos\varphi_n \\ &\quad - \zeta \cdot \sin\varphi_n) \cdot d\varepsilon. \end{aligned} \tag{5}$$

Therefore, in our case, the projection operator is completely defined by the synchrotron phase φ. For the computer calculations the continuous functions need to be represented by a discrete set of data points. Let us consider that we have a distribution function defined on an $N \times N$ grid in the phase space, $F = [f_{il}]$. Our goal is now to find a way to extract information about the array F from the finite number of projections.

We obtain our full set of linear projections from a dual-sweep streak camera, which captures the synchrotron radiation emitted by the electrons. A frame grabber digitizes the images from the streak camera. Let us select a subset of J profiles (along vertical lines in Fig. 1), which cover a small portion of a synchrotron period, and use M pixels from each image. The information contained in these projections has $J \times M$ data points. The matrix form of Eq. (2) takes the following form:

$$[I]_u = [P]_{u,v} \cdot [A]_v, \qquad u = N^{2D}, \qquad v = M \cdot J, \tag{6}$$

where the array I is a combination of ordered J projections, F is the array of ordered f_{il}, and P is the projection matrix. In the 2-dimensional case, Eq. (6) takes the form

$$\begin{pmatrix} I_{j=1,m=1} \\ \vdots \\ I_{1,M} \\ I_{2,1} \\ \vdots \\ I_{J,M} \end{pmatrix} = \begin{pmatrix} P_{1,1,1} & \cdots & & \cdots & P_{1,1,\alpha} \\ \vdots & \ddots & \vdots & \iddots & \vdots \\ P_{1,M,1} & \cdots & & \cdots & P_{1,M,\alpha} \\ \vdots & \iddots & \vdots & \ddots & \vdots \\ P_{J,M,1} & \cdots & & \cdots & P_{J,M,\alpha} \end{pmatrix} \begin{pmatrix} a_1 \\ \vdots \\ \\ \vdots \\ a_\alpha \end{pmatrix}. \tag{7}$$

In Eq. (7), the array I represents the given set of profile data, the matrix P, the projection matrix, is calculated by geometric considerations, i.e., the projection of a set of basis functions (particular instances of which follow) onto the pixels of the detection image, and the matrix A represents the amplitudes of the basis functions.

In the case of the giant pulse process in a storage ring FEL, the relevant parameter for the projection matrix is the synchrotron phase, which can be found from the synchrotron frequency and the detection time of each projection.

The problem is now reduced to a method of solving Eq. (2) and finding F with reasonable accuracy. The projection matrices are typically very large, nonsquare and sometimes singular, which makes the singular value decomposition (SVD) method a natural choice for solving Eq. (2).

B. SVD

There is a wealth of information concerning SVD (see for instance [8]), but it is, in brief, the decomposition which, when inverted, satisfies the least-squares minimum criteria for the function

$$\Phi = \|I - P \cdot F\|^2. \tag{8}$$

One decomposes a matrix $P \rightarrow UDV^T$, where the columns of U are the eigenvectors of PP^T, the columns of V are the eigenvectors of $P^T P$, and D is a diagonal matrix comprising the singular values (square root of the eigenvalues) of PP^T. U and V are, by definition, orthogonal. This decomposition can be inverted (pseudoinverse) as $P^+ = VD^+U^T$, where the diagonal of D^+ is made up of the reciprocal of each of the singular values in D, σ_k, in descending order, so long as the singular value in question is not zero. If the singular value of D is zero, then the corresponding element of D^+ is also zero. If we assume P is a $u \times v$ matrix, and then as v increases, some values of

D^+ can be very large, and undue emphasis can be put on the corresponding singular values. This may cause a very high sensitivity of the method to errors and noise. Fortunately, SVD allows us to truncate the sum at any desirable number of eigenvalues (which are all positive, or zero) with any $K \leq \min(u, v)$:

$$P^+ = \sigma_1 E_1 + ..\sigma_K E_K = \sum_{k=1}^{K} \sigma_k E_k; \qquad E_k = |U_k\rangle\langle V_k|, \tag{9}$$

where the last quantity indicates an outer product. Truncation provides for the robustness of this method, and makes it less sensitive to errors in calculation of the projection matrix as well as errors from the imaging process. The projection matrix is defined by the type of projection (e.g., angle of rotation), the size of the pixel in the image array, and the type of discrete representation of a continuous distribution. In the following sections we will present four models of discrete representation: pillbox, Gaussian, Hermite-Gaussian, and Laguerre-Gaussian.

C. Pillbox representation

This is a representation of the distribution by $N \times N$ pillboxes with F_{il} height located on an evenly spaced 2D grid.

The elements of the projection matrix are equal to the area of intersection of a box located on an (i, l) grid node with the lines indicating the boundaries of the mth pixel. The grid rotates around the origin according to the angle φ of the given projections. This is illustrated in Fig. 2.

$$P_{j*m,N^2(i-1)+l} = \text{Area}_{\text{overlap}}. \tag{10}$$

The pillbox representation has the advantage of giving the exact projection matrix, but the sharp corners inherent in the method do not allow for a smooth reconstruction. Because of the high level of sensitivity intrinsic in SVD, these sharp corners can be highly exaggerated in the reconstruction.

D. Gaussian representation

A more elegant representation of the distributed function is the use of $N \times N$ Gaussians centered on the nodes of the 2D grid [see Eq. (11a)]. Each Gaussian has individual height F_{il} for (i, l)th node and common rms width σ_r, which plays the role of an adjustable parameter. The projection matrix is then found by projecting each Gaussian mode onto each pixel using Eq. (6) and the pixel width (w_m, w_{m+1}):

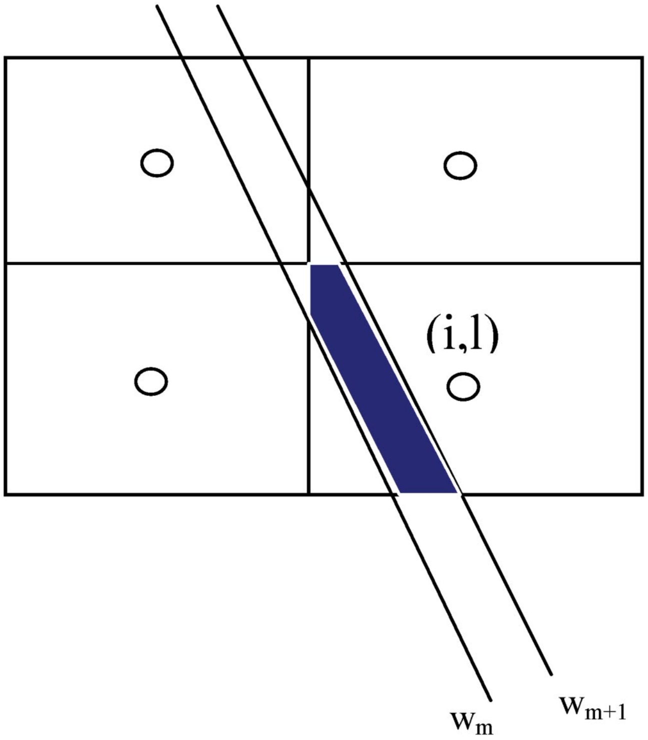

FIG. 2. (Color) Element $P_{j*m,N^2*(i-1)+l}$, the projection of grid-box (i, l) onto the mth pixel at angle φ, is equal to the shaded area of intersection.

$$F(x, y) = \sum_{i.l} F_{i,l} e^{-(1/2\sigma_{\text{rep}}^2)[-(x-x_l)^2-(y-y_i)^2]}, \tag{11a}$$

$$(b) P_{j,l,N^2(i-1)+l} = \sqrt{2\pi}\sigma_r \int_{w_m}^{w_{m+1}} e^{-\frac{1}{2\sigma_r^2}(x_l \cos\varphi_j + y_i \sin\varphi_j - u)} du. \tag{11b}$$

E. Special function method

The most elegant representation of the distributed function is the use of higher-order Gaussian modes, each of which has amplitude F_{kl} for (k, l)th mode:

$$F(x, y) = \sum_{k,l} A_{k,l} \times \chi_{k,l}(x, y), \tag{12a}$$

$$P_{j,m,\alpha(k-1)+l} = \int_{-\infty}^{\infty} \chi_{k,l}(x', y') dy, \quad x' = x\cos\varphi_j + y\sin\varphi_j; y' = x\sin\varphi_j - y\cos\varphi_j \tag{12b}$$

where χ_{kl} are the basis vectors for the problem and α is the number of basis functions used for the representation of the distribution. The two relevant basis functions are that of the Hermite-Gaussian and Laguerre-Gaussian functions [9]:

$$HG_{k,l}(\lambda x, \lambda y) = H_k(\lambda x)H_l(\lambda y)e^{-\lambda^2(x^2+y^2)}; \tag{13a}$$

$$LG^{\pm l}_{l+2k}(\lambda x, \lambda y) = N_{k,l}L^l_k[\lambda^2(x^2+y^2)][\lambda^2(x^2+y^2)]^{l/2}e^{-\lambda^2(x^2+y^2)}e^{\pm il\theta}; \qquad N^l_k = \frac{(-1)^k}{\sqrt{\pi}}\sqrt{\frac{k!}{(l+k)!}}; \qquad \theta = \tan^{-1}\left(\frac{y}{x}\right) \tag{13b}$$

The solution for Eq. (12b) is simple for both (13a) and (13b) and [1]; it is

$$\begin{aligned} &(13a) \rightarrow P_{j,m,\alpha*(k-1)+l} = \frac{\sqrt{\pi}}{\lambda}(\cos\phi)^k(\sin\phi)^l e^{-\lambda^2p^2}H_{k+l}(\lambda p);\\ &(13b) \rightarrow P_{j,m,\alpha*(k-1)+l} = N1_{kl}e^{\pm il\phi}e^{-\lambda^2p^2}H_{l+2k}(\lambda p);\\ &N1_{kl} = \sqrt{\frac{1}{k!(l+k)!}}\frac{1}{2^{l+2k}}; \qquad p = x\cos\phi + y\sin\phi \end{aligned} \tag{14}$$

The straightforward solution of the elements of the projection matrix for these representations makes them particularly attractive, as it speeds up the computation time considerably. The functions H and L are the Hermite and associated Laguerre polynomials, respectively. λ is an adjustable parameter. The most obvious advantage of using the higher-order Gaussian modes is that they form a complete representation of our function space. The H-G functions also can be easily generalized into an N-dimensional problem, however, the L-G functions work only for the two-dimensional case.

F. Solution

When the projection matrix is pseudoinverted for a given choice of K (i.e., cutoff number of eigenvectors used in reconstruction) using Eq. (9), the $P^+(K)$ gives the resulting elements of A_{kl} as

$$[A] = [P^+(K)][I]. \tag{15}$$

In the pillbox case these are the heights of the boxes on the grid with discontinuities on each grid edge. For the Gaussian representation, the result is a smooth function (11a), whose scale of variations can be limited by increasing σ_r. The increase of σ_r to a value at or above the size of a grid node will lead to a reduction in the accuracy of the representation; hence, there is an optimum s_r, which provides a smooth but reasonably accurate representation of the real distribution function. In the case of higher-order Gaussian modes, the solutions of (15) are the amplitudes of the modes, and are inserted into (12a). The choice of basis should depend on the nature of the distribution function.

III. THEORETICAL COMPARISON

In order to study the theoretical aspects of the four representations, we created a theoretical construction, wherein we may compare a known function with our reconstruction. Here we present a few selected results that employ as a trial function

$$F(x, y) = x^2 * y * e^{-(1/2\sigma^2)(x^2+y^2)}. \tag{16}$$

This function is graphed in Fig. 3.

The pillbox and Gaussian representations use a 13 × 13 2D grid, while the Laguerre-Gaussian and Hermite-Gaussian representations use a 51 × 51 grid for the purposes of reconstruction (note that the higher-order Gaussian mode representations are not dependent on phase-space resolution, i.e., we can make the phase space as fine as we like). The theoretical profiles created from the known function have a size of 51 pixels. We used the SVD method described above for all representations, and then evaluated the accuracy of the reconstruction by subtracting the theoretical numbers from the reconstruction on the grid and comparing the norm of the difference with the norm of the original function:

$$\text{Error}\,[\%] = \frac{\sum_{i,l}|F(i,l) - F_{\text{reconstructed}}(i,l)|}{\sum_{i,l}F(i,l)} * 100. \tag{17}$$

The theoretical object we are trying to reconstruct cannot be represented by any of the above representations

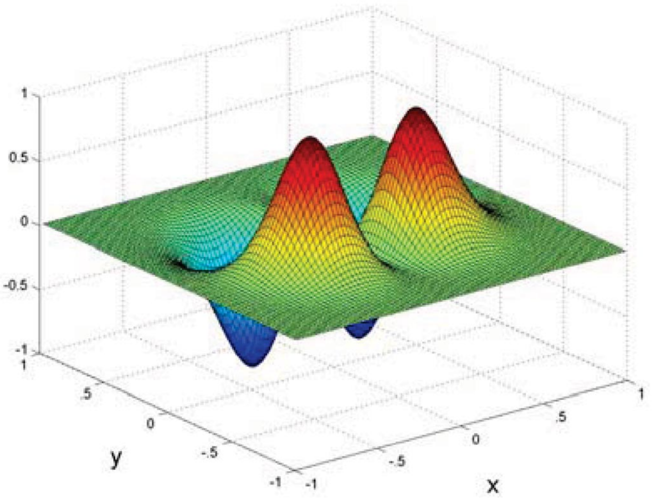

FIG. 3. (Color) The function in Eq. (16). It is a function with negative amplitudes that cannot be represented completely by any of the above representations without using an infinite number of basis functions, so it provides a good test of the method.

without using an infinite number of basis functions, so it is not possible to get a perfect reconstruction for this object. One way to analyze the success of each representation is by comparing the error versus the number of profiles used in reconstruction for all four representations. Figure 4 shows the results of this analysis for our model distribution for each representation.

Several important conclusions can be drawn from Fig. 4. First, the pillbox and Gaussian representation do not give an accurate reconstruction of this object. Both the Laguerre-Gaussian and Hermite-Gaussian representations, however, give very accurate reconstructions of this object, even given only two profiles. These conclusions are consistent with other results of our work [10]. In fact, the Laguerre-Gaussian representation consistently gives us the best results for reconstructing two-dimensional objects. The fact that it reconstructs the object given only two profiles is a true measure of success for this method. The reconstruction of the theoretical object using the Laguerre-Gaussian representation and two profiles is shown in Fig. 5. It is nearly identical to Fig. 3.

IV. ANALYSIS OF GIANT PULSES

Figure 1 shows an example of the measured dual-sweep streak-camera images of electron beam evolution in the Duke OK-4 storage ring FEL during the giant pulse process. During the above measurement the synchrotron frequency was 24.3 kHz, and the image shows the evolution of the longitudinal distribution of the electron beam over approximately 12 synchrotron oscillations. One can see that there is a transition region, where the length of the e-bunch is evolving rapidly, and dramatically, in less than one synchrotron oscillation.

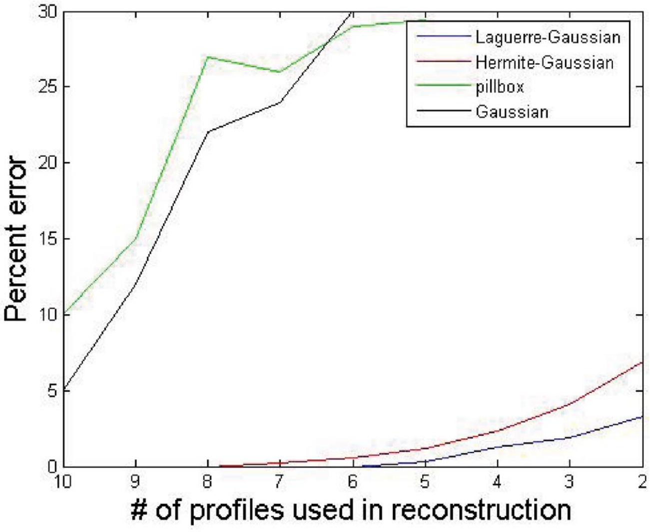

FIG. 4. (Color) Percent error vs number of profiles for pillbox, Gaussian, Laguerre-Gaussian, and Hermite-Gaussian representation for a theoretical shape given by Eq. (16), each profile is separated by 10°.

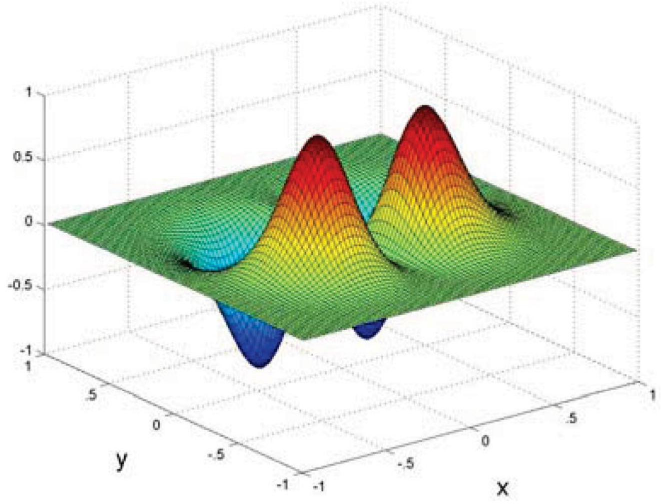

FIG. 5. (Color) A reconstruction of the theoretical object using the Laguerre-Gaussian representation with two profiles. The error between this reconstructed object and the theoretical object is 3.3%.

The self-consistent theory of giant pulses [11] predicts strongly asymmetric, snail-like distribution [12] generated in the giant pulse process. Our new method allows us to reconstruct distributions from a limited number of profiles, to observe the details of phase-space dynamics during the giant pulse and to compare them to the theory. Preliminary results look promising, as seen in Figs. 6–9 below where the Laguerre-Gaussian representation was used with only two streak-camera profiles for the longitudinal phase-space reconstruction of the electron beam in giant pulse mode. Figure 6 shows the longitudinal phase-space reconstruction

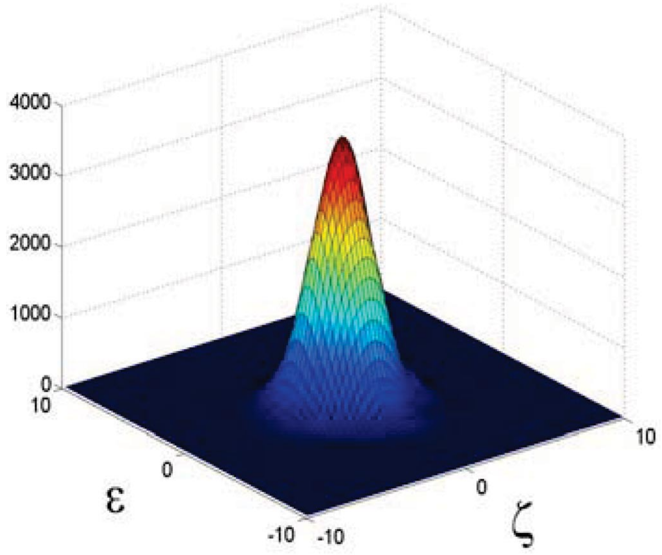

FIG. 6. (Color) Longitudinal phase-space reconstruction of *E* beam in equilibrium (turn 100, before lasing) using 2 profiles, 6.82° apart. Scale is in normalized units indicated in Eq. (3).

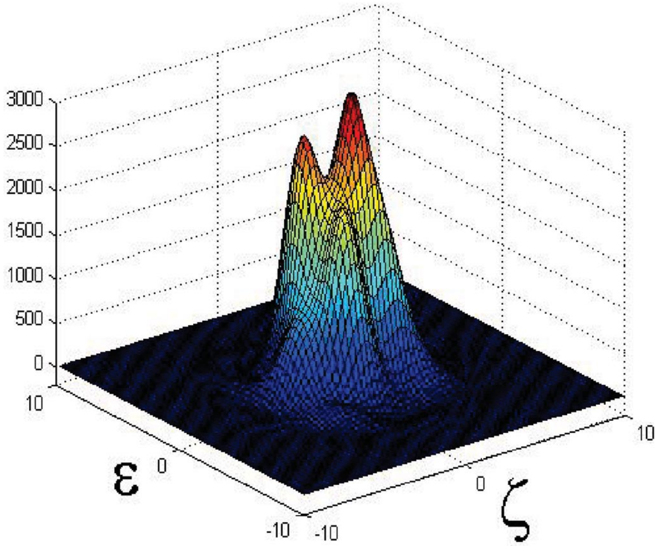

FIG. 7. (Color) A longitudinal phase-space reconstruction of E beam in giant pulse mode using 2 streak-camera profiles, 6.82° apart, in the transition region (turn 225). Noticeable double hump and hot spot at $\epsilon < 0$ and $\zeta = 0$ is remarkably similar to prediction of theory in 10,11.

at turn 100, when the E beam has its equilibrium energy spread, Figs. 7 and 8 correspond to longitudinal phase-space reconstructions of the E beam in the transition region (turns 225 and 240). Figure 9 shows a longitudinal phase-space reconstruction of the E beam at turn 280, at about the time the lasing reaches saturation.

All of the above longitudinal phase-space reconstructions were performed using only two streak-camera profiles (separated by a synchrotron phase of 6.82°, or 1.52 μs), which is a significant triumph for this method.

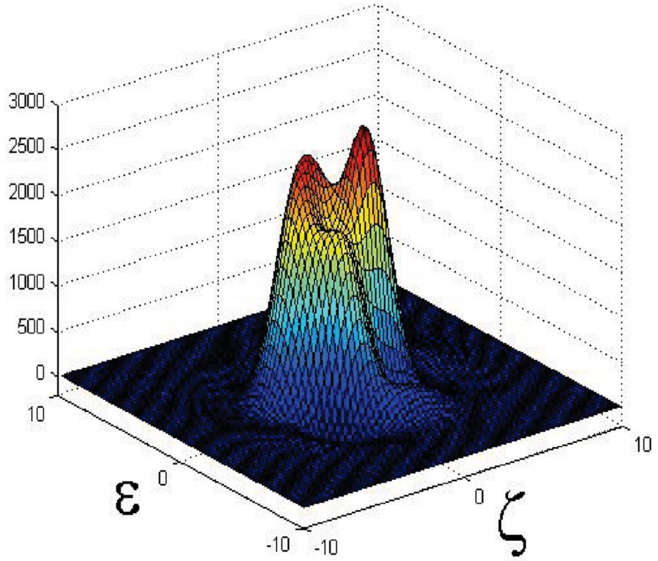

FIG. 8. (Color) Longitudinal phase-space reconstruction of the electron beam in giant pulse mode at turn 240.

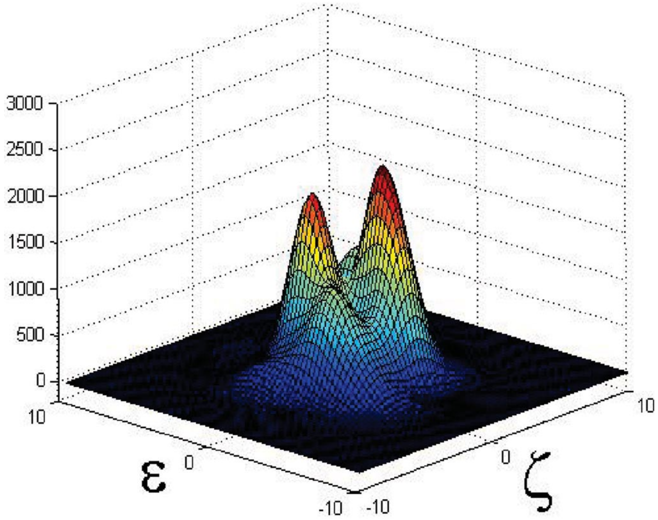

FIG. 9. (Color) Longitudinal phase-space reconstruction of the electron beam in giant pulse mode at turn 280. The distribution has separated into two distinct peaks, indicating the "burning out" of electrons at $\zeta = 0$.

Qualitatively, they compare very favorably with predictions from numerical simulations [10]. Also, the fact that no negative amplitudes are allowed into the reconstructions (the streak-camera data points are always positive) is another good sign that the method is working. The Laguerre-Gaussian representation is a particularly good choice for these reconstructions because of its cylindrical symmetry. The other representations require more profiles for the reconstructions, and the results are not nearly as good.

V. CONCLUSIONS

We developed a method of phase-space reconstruction that requires only a full set of two or more linear profiles. Theoretical models indicate that, with limited resolution, we can get a good reconstruction (error <5%) with a set of two profiles. We used experimental data from giant-pulse measurements at the Duke storage ring FEL to test the model, and saw very favorable results.

It is important that this method works for any linear profiles, not only for rotations [5]. It has potential applications for accelerator physics, medicine, military, and astronomy. Future work will be to further improve the model, compare it to giant-pulse simulations, and apply the method to other problems.

[1] S. R. Deans, *The Radon Transform and Some of Its Applications* (Wiley & Sons, New York, 1983).
[2] A.Rosenfeld and A.Kak, *Digital Picture Processing* (Academic Press, Orlando, FL, 1982).
[3] M. Huning III, in DIPAC 2001 Proceedings, ESRF, Grenoble, France, pp. 56–60.

[4] I. V. Pinayev *et al.*, Nucl. Instrum. Methods Phys. Res., Sect. A **475**, 222 (2001).
[5] K.Chalut and V. N. Litivinenko, "SVD-Bbased Tomography" (to be published).
[6] A. H. Lumpkin *et al.*, Nucl. Instrum. Methods Phys. Res., Sect. A **407**, 338 (1998).
[7] See, for example, Philip J. Briant and Kjell Johnsen, *The Principles of Circular Accelerators and Storage Rings* (Cambridge University Press, Cambridge, England, 1993), p. 156.
[8] P. E. Gill *et al.*, *Numerical Linear Algebra and Its Optimization* (Addison-Wesley, Reading, MA, 1989).
[9] G. Arfken and H. Weber, *Mathematical Methods for Physicists* (Academic Press, San Diego, CA, 1995), 4th ed.
[10] K. Chalut, Ph.D. thesis, Duke University, 2005.
[11] V. N. Litvinenko, in *Proceedings of FEL Conference, 2002*, edited by K.-J. Kim, S. V. Milton, and E. Gluskin (APS, Argonne, IL, 2002).
[12] V. N. Litvinenko *et al.*, Nucl. Instrum. Methods Phys. Res., Sect. A **358**, 334 (1995).